ARTICLE

Optimization of the structural characteristics of CaO and its effective stabilization yield high-capacity CO_2 sorbents

Muhammad Awais Naeem[1], Andac Armutlulu [1], Qasim Imtiaz[1], Felix Donat[1], Robin Schäublin[2], Agnieszka Kierzkowska[1] & Christoph R. Müller[1]

Calcium looping, a CO_2 capture technique, may offer a mid-term if not near-term solution to mitigate climate change, triggered by the yet increasing anthropogenic CO_2 emissions. A key requirement for the economic operation of calcium looping is the availability of highly effective CaO-based CO_2 sorbents. Here we report a facile synthesis route that yields hollow, MgO-stabilized, CaO microspheres featuring highly porous multishelled morphologies. As a thermal stabilizer, MgO minimized the sintering-induced decay of the sorbents' CO_2 capacity and ensured a stable CO_2 uptake over multiple operation cycles. Detailed electron microscopy-based analyses confirm a compositional homogeneity which is identified, together with the characteristics of its porous structure, as an essential feature to yield a high-performance sorbent. After 30 cycles of repeated CO_2 capture and sorbent regeneration, the best performing material requires as little as 11 wt.% MgO for structural stabilization and exceeds the CO_2 uptake of the limestone-derived reference material by ~500%.

---

[1] Department of Mechanical and Process Engineering, Laboratory of Energy Science and Engineering, ETH Zurich, Leonhardstrasse 21, 8092 Zurich, Switzerland. [2] Scientific Center for Optical and Electron Microscopy, ETH Zurich, Auguste-Piccard-Hof 1, 8093 Zurich, Switzerland. Correspondence and requests for materials should be addressed to C.R.Mül. (email: muelchri@ethz.ch)

CO$_2$ capture and storage (CCS) is one of the technologies that have been proposed to mitigate climate change stemming primarily from the ever-increasing anthropogenic CO$_2$ emissions[1–6]. At present, the capture of CO$_2$ by amine scrubbing is a well-established process and industrially applied for the purification of natural gas; yet, it is associated with high costs[7] and potentially adverse environmental effects through the formation of harmful side-products such as nitrosamines and nitramines[8,9].

Viable alternatives to amine scrubbing are solid CO$_2$ sorbents such as calcium oxide (CaO)[10–15]. The so-called calcium looping process utilizes CaO as a CO$_2$ sorbent, and among its most advantageous characteristics are (i) the low cost and wide availability of naturally occurring, environmentally benign CaO precursors (e.g., limestone and dolomite), (ii) the potential use of deactivated material in the cement industry, (iii) the high CO$_2$ capture capacity of CaO ($\sim$0.78 g$_{CO_2}$/g$_{CaO}$), and (iv) the fast kinetics of the underlying capture and release reaction[10–12]:

$$CaO_{(s)} + CO_{2(g)} \leftrightarrow CaCO_{3(s)} \quad (\Delta H^{\circ}_{298K} = \pm 178\,kJ\,mol^{-1}) \quad (1)$$
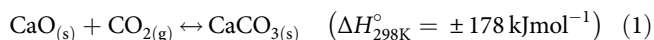
However, the main drawback associated with limestone-derived CaO is its low cyclic stability owing to the sintering-induced deterioration of the microstructure of as-derived CaO. Indeed, the Tammann temperature (T_T) of CaCO$_3$ ($\sim$530 °C), a measure for the onset of sintering, is well below the operating temperatures of calcium looping[11], i.e., 600–700 °C for carbonation (CO$_2$ capture step) and 900 °C for calcination (regeneration step).

One of the approaches that have been attempted to reduce the sintering-induced capacity decay of CaO-based CO$_2$ sorbents is the incorporation of high-T_T stabilizers such as Al$_2$O$_3$, MgO, TiO$_2$, or ZrO$_2$ which are typically inactive for CO$_2$ capture. Several works have demonstrated that the utilization of such stabilizers can improve appreciably the cyclic CO$_2$ uptake of CaO[10–12,16–21]. In general, stabilizers can be grouped into two categories: (i) the ones that form a solid solution with CaO (e.g., Al$_2$O$_3$ that can yield Ca$_{12}$Al$_{14}$O$_{33}$ or Ca$_9$Al$_6$O$_{18}$, or ZrO$_2$ forming CaZrO$_3$), and (ii) the ones that do not form a solid solution under relevant operating conditions (e.g., MgO or Y$_2$O$_3$). Although Al$_2$O$_3$ has received arguably the highest attention so far, the latter group of stabilizers is potentially more attractive in terms of preserving the intrinsically high CO$_2$ uptake of CaO, as active CaO is not "consumed" through the formation of a solid solution that is inactive for CO$_2$ capture[22]. Furthermore, a recent study focusing on the deactivation mechanism of Ca$_3$Al$_2$O$_6$-stabilized, CaO-based CO$_2$ sorbents demonstrated the segregation of Al$_2$O$_3$ from Cal-Al mixed oxides, leading to a sintering-induced structural collapse of the material after a certain number of cycles[23]. Hence, considering also its high T_T (i.e., $\sim$1290 °C), MgO is an attractive structural stabilizer. In addition, similar to CaO, MgO is inexpensive and environmentally benign[24].

The effective incorporation of a stabilizer into a porous CaO structure relies on two key aspects: (i) its homogeneous distribution within the CaO matrix on a nanometer or even atomic level, and (ii) the minimization of its quantity to maintain a high fraction of CaO in the material. However, it is also worth noting that several reports have indicated that the presence of a stabilizer per se is not sufficient to realize sorbents featuring both cyclic stability and a high CO$_2$ uptake capacity[12,19,25]. Indeed, also the structure of CaO has to meet certain characteristics, such as being composed of small building blocks typically in the form of nanometer-sized particles/grains[11,20,25]. As in the case of most non-catalytic gas-solid reactions, the carbonation of CaO can occur in two consecutive regimes, i.e., an initial, rapid, kinetically controlled reaction stage that is followed by a relatively sluggish conversion stage. The latter reaction stage is controlled by diffusive limitations, first owing to migration of CO$_2$ through the network of pores and later the growth of a CaCO$_3$ product layer that has significantly poorer diffusion characteristics for CO$_2$ when compared to CaO ($D_{CaO}/D_{CaCO_3} \approx 100$)[23,26,27]. Considering the relatively short residence times in practical fluidized bed reactors, it is therefore essential that CO$_2$ capture is performed largely in the kinetically controlled regime. This can be achieved by ensuring a nano-structured morphology of CaO, minimizing the diffusion lengths of CO$_2$ through the freshly formed CaCO$_3$ layer. Previous, albeit indirect, measurements have indicated a critical product layer thickness (i.e., the thickness of the product layer when the reaction becomes diffusion limited) of $\sim$50 nm[28,29]. Furthermore, the CO$_2$ sorbent should possess a certain level of porosity in order to be able to compensate for the large volumetric changes that occur during cyclic operation, as the molar volume of CaCO$_3$ is more than twice as high as that of CaO.

Previous studies aiming at developing stabilized, CaO-based CO$_2$ sorbents have utilized various synthesis methods, including wet-mixing[30,31], precipitation[32], co-precipitation[33], sol–gel[34], flame spray pyrolysis[35], and re-crystallization[22]. Yet, the majority of these works have fallen short of ensuring a structure that meets all of the essential characteristics outlined above. An additional concern is that some works that have reported an attractive CO$_2$ uptake, have tested the materials under unrealistic operating conditions (e.g., regeneration in pure N$_2$ at temperatures <900 °C)[36], or are based on synthesis protocols that rely on environmentally harmful precursors[17,37–39].

Recently, template-assisted synthesis approaches have been adopted to realize hollow microspheres and nanospheres for a plethora of applications, including catalysis, energy storage, drug delivery etc.[40,41]. These templates, being either hard (e.g., silica, carbon) or soft (e.g., micelles, emulsions), are coated via techniques that typically involve the precipitation of inorganic precursors onto their surface or the layer-by-layer assembly of inorganic particles[42,43]. The final structure, obtained after the selective removal of the template via dissolution, etching or thermal decomposition, is composed of a hollow interior that is contained by an often mesoporous shell[44]. To limit the complexity and to increase the throughput of the synthesis procedure, a favorable approach would involve the simultaneous formation of the template and the precipitation of the compound(s) of interest.

Herein, we report a facile, template-assisted synthesis approach to yield a highly effective, MgO-stabilized, CaO-based CO$_2$ sorbent that relies on environmentally benign precursors. The synthesis protocol adopted here features the aforementioned desirable one-pot characteristics. Carbonaceous spheres, formed in situ from a xylose precursor during hydrothermal synthesis, act hereby as a template and encapsulates compounds of Ca and Mg that are precipitated simultaneously via the hydrolysis of urea. Thermal removal of the template yields hollow microspheres with highly porous shells. The resultant structures contain all of the key features that are essential to yield a CaO-based sorbent with a high and cyclically stable CO$_2$ uptake. After 30 cycles of calcination and carbonation under "harsh" operating conditions, the CO$_2$ uptake of the materials synthesized is 0.50 g$_{CO_2}$/g$_{sorbent}$ (equivalent to a capacity retention of 83%), exceeding the capacity of the benchmark limestone by almost 500%.

Results

Synthesis of the CO$_2$ sorbents. As illustrated schematically in Fig. 1, the hydrothermal treatment of an aqueous solution of xylose, urea, and glycine together with Ca and Mg precursors at
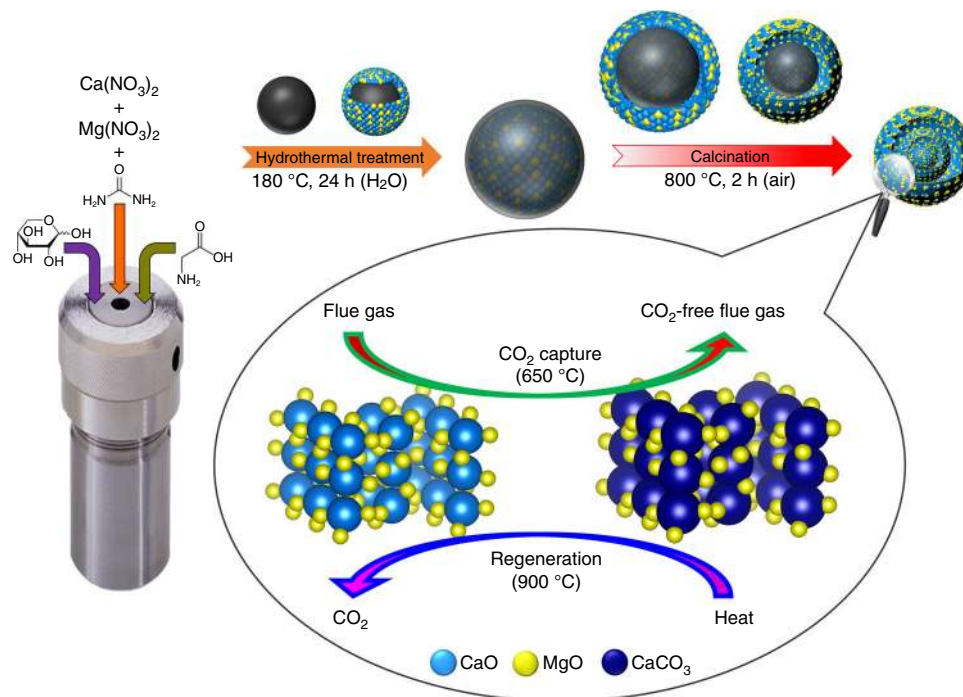
Fig. 1 Synthesis protocol. Schematic illustration of the hydrothermal approach developed here to synthesize template-assisted, MgO-stabilized, CaO-based CO_2 sorbents

180 °C for 24 h yielded micron-sized carbonaceous spheres that encapsulate homogeneously Ca^{2+} and Mg^{2+} species. The simultaneous hydrolysis of urea led to a gradual rise in the pH resulting in the precipitation of $CaCO_3$ and $MgCO_3$[45–47]. EDX analysis of FIB cross-sections of the as-synthesized material (Supplementary Fig. 1) confirms the homogeneous distribution of Ca and Mg within the carbonaceous template, a rather surprising observation. The presence of glycine in the precursor solution yields complexes of Ca^{2+} and Mg^{2+} which improves the homogeneity of the precipitated $CaCO_3$ and $MgCO_3$ structures[48]. Xylose was preferred over alternative biomass precursors (e.g., glucose or sucrose), since hydrothermally treated pentoses (e.g., xylose) were shown to yield highly dispersed carbonaceous spheres, whereas the hydrothermal treatment of hexoses (e.g., glucose) resulted typically in an interconnected network of carbonaceous spheres[49]. Calcination of the materials in air at 800 °C resulted in the complete removal of the carbonaceous template and the formation of highly porous, multishelled microspheres, whereby the shells are composed of CaO and MgO nanoparticles. It is noteworthy that all of the compounds utilized in the synthesis of the sorbents are relatively inexpensive and environmentally benign as opposed to other commonly used template-assisted approaches that involve, e.g., resorcinol/formaldehyde-derived templates[50].

Here, we synthesized CO_2 sorbents with four different molar ratios of Ca:Mg (i.e., 100:0, 90:10, 85:15, and 80:20). The ratio of Ca to Mg in the materials was determined by ICP-OES, and it was confirmed that the Ca:Mg ratio of the precursors introduced to the reaction vessel was conserved largely throughout the synthesis (Table 1). According to our ICP-OES data, the sorbents Ca90Mg10, Ca85Mg15, and Ca80Mg20 had a MgO content of 8, 11, and 16 wt.%, respectively. These quantities of stabilizers were significantly lower than what has been used so far in most CaO-based CO_2 sorbents as reported in the literature[11,51]. To achieve a high CO_2 uptake capacity (on a weight basis), it is essential to minimize the quantity of the CO_2-inactive stabilizer in the sorbent.

Table 1 Composition of the CO_2 sorbents synthesized and the crystallite sizes of MgO and CaO as determined by ICP-OES and XRD, respectively

Sorbent	Ca:Mg (molar ratio)[a]	CO_2-active material content (wt.%)[b]	Crystallite size (nm)[c]	
			CaO (200)	MgO (200)
Ca90Mg10	8.9:1.0	~92	43	22
Ca85Mg15	8.5:1.5	~89	45	21
Ca80Mg20	7.8:2.0	~84	46	24

[a]Determined by ICP-OES
[b]Determined by Rietveld refinement
[c]Calculated by the Scherrer Eq. (2) using the XRD data of freshly calcined samples

Effect of synthesis method on the performance of the sorbents

Structural characterization of the sorbents. Electron microscopy images of the synthesized materials shown in Fig. 2 reveal that after the thermal removal of the carbonaceous template the desired structure was obtained, i.e., hollow, micrometer-sized spheres composed of highly porous shell(s). Both SEM and TEM images of the samples confirm that variation of the molar ratio of Ca:Mg did not have a noticeable impact on the overall morphology of the materials. The average size of the shell-comprising CaO nanoparticles was determined as ~85 ± 20 nm (Supplementary Fig. 2), i.e., <100 nm, hence fulfilling an essential requirement to avoid (or at least minimize) diffusion limitations during the CO_2 capture reaction. The average particle size of MgO was measured as 24 ± 5 nm.

The presence of a porous shell is critical as it allows a rapid transport of CO_2 to and from the material, whereas the central void provides the required volume to accommodate the large volumetric changes the material undergoes during CO_2 capture and regeneration cycles. Furthermore, the physical separation of the individual nanoparticles is expected to mitigate effectively
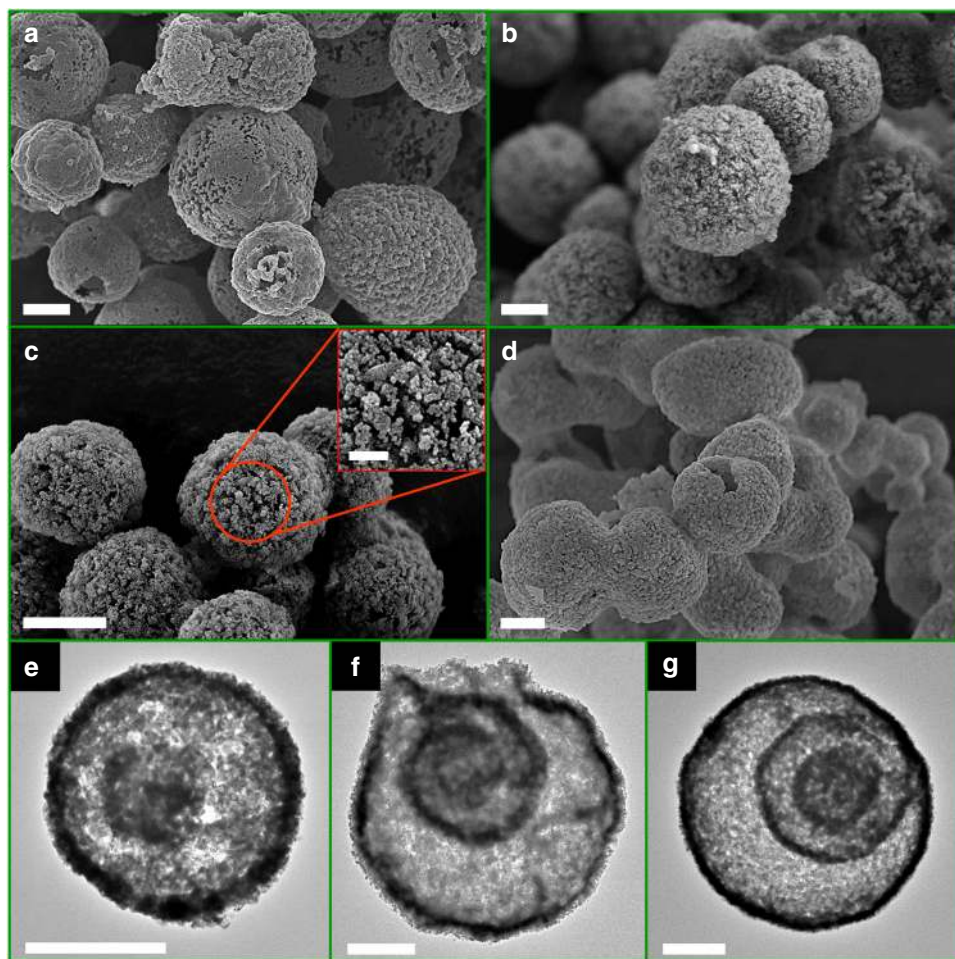
Fig. 2 Formation of porous multishelled structures. SEM and TEM images of the hydrothermally synthesized sorbents after thermal removal of the carbonaceous template. **a**, **e** Ca100Mg0. **b**, **f** Ca90Mg10. **c**, **g** Ca85Mg15. **d** Ca80Mg20. Scale bars: 1 μm for **a**–**g**, and 200 nm for inset, respectively
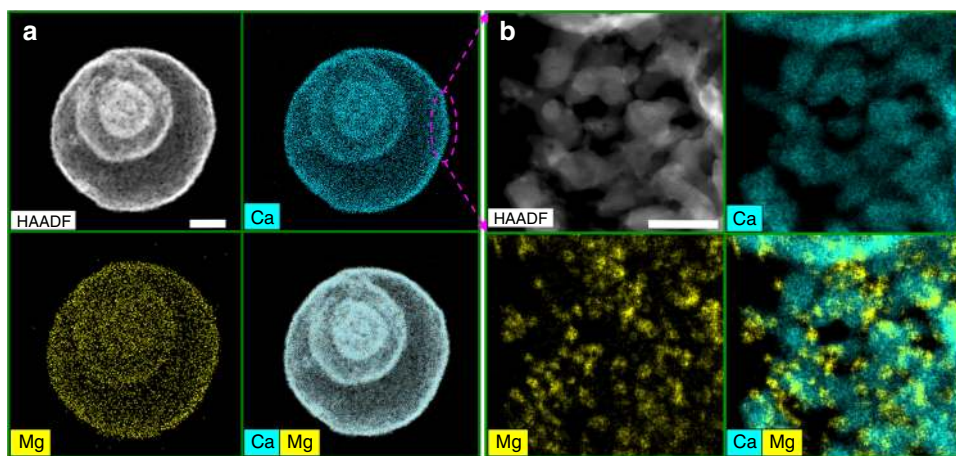

Fig. 3 Compositional homogeneity. **a**, **b** Low-magnification and high-magnification HAADF-STEM images of Ca85Mg15 along with EDX elemental mapping showing the distribution of Ca and Mg in the sorbents following the thermal removal of the template, respectively. Scale bar: 1 μm in **a**, and 200 nm in **b**, respectively

particle/grain agglomeration[12]. An advantage of the multishelled architecture is an increased packing density (as compared to a single-shelled material), providing, thus, a higher density of CO_2-active material per volume without significantly compromising the availability of void space[52].

To evaluate the compositional homogeneity between CaO and MgO, a feature that is critical to ensure a high thermal stability of the material, HAADF-STEM with EDX analyses were carried out. Figure 3 and Supplementary Fig. 3 show the elemental mappings of Ca and Mg of a multishelled microsphere. Indeed, a

homogeneous distribution of MgO within the CaO matrix is observed for both Ca90Mg10 and Ca85Mg15. The high-magnification STEM image complemented by EDX maps (Fig. 3) and the TEM image of the sample (Supplementary Fig. 4) reveal the presence of MgO in the form of uniformly dispersed nanoparticles on the CaO surface. The homogeneous mixing between the active phase and the stabilizer on the nanometer scale is a key requirement for the effective structural stabilization of the sorbent during the cyclic operation, since the functionality of the inert stabilizer (i.e., MgO; T_T ~1290 °C) is to act as a physical "barrier" between neighboring CaO/CaCO$_3$ particles. Such a barrier effectively prevents the agglomeration of the CaO (or CaCO$_3$) particles and hence avoids a transition to the diffusion-limited CO$_2$ uptake.

XRD measurements, plotted in Fig. 4a, reveal that after the removal of the carbonaceous template, the materials were composed primarily of CaO and MgO. The presence of Ca(OH)$_2$ is owing to the highly hygroscopic nature of CaO, whereas CaCO$_3$ is believed to form due to the release of CO$_2$ during the thermal decomposition of the carbonaceous templates. Rietveld analysis of the sorbents (Supplementary Fig. 5) further confirms that there is no solid solution between CaO and MgO after the thermal removal of the template at 800 °C, suggesting that the homogeneous mixing between the CaO and MgO phases is a purely "physical" phenomenon. Moreover, the crystallite sizes of CaO and MgO, calculated from the XRD data using the Scherrer equation (Eq. 2)

(Table 1), indicate that the introduction of MgO does not have a notable impact on the crystallite size of CaO.

Assessment of the CO$_2$ capture performance of the sorbents. The cyclic CO$_2$ capture performance of the sorbents was evaluated in a TGA and compared to the benchmark sorbent, i.e., CaO derived from limestone. In order to comply with the practically relevant operation conditions, calcination was performed at 900 °C in a CO$_2$ atmosphere, and a rapid temperature ramp of 50 °C min^{-1} was applied between the carbonation and calcination temperatures. For an initial assessment, ten cycles were performed. Already from these initial tests, it is clear that all of the hydrothermally synthesized CO$_2$ sorbents show a better performance than the benchmark limestone that underwent significant sintering during cyclic testing (Fig. 4b). In particular, the MgO-containing sorbents exhibit a stable CO$_2$ uptake, whereas CaO synthesized in the absence of a stabilizer (i.e., Ca100Mg0) reveals a characteristic decay in the CO$_2$ uptake with cycle number (Fig. 4c). This observation is a clear indication of the structural stabilizing effect of MgO. The fact that hydrothermally synthesized CaO without any stabilizer (Ca100Mg0), i.e., a material that initially features structures with favorable CO$_2$ capture characteristics, significantly outperforms the limestone-derived benchmark supports the underlying hypothesis that the particular structure of CaO, i.e., being composed of primary particles
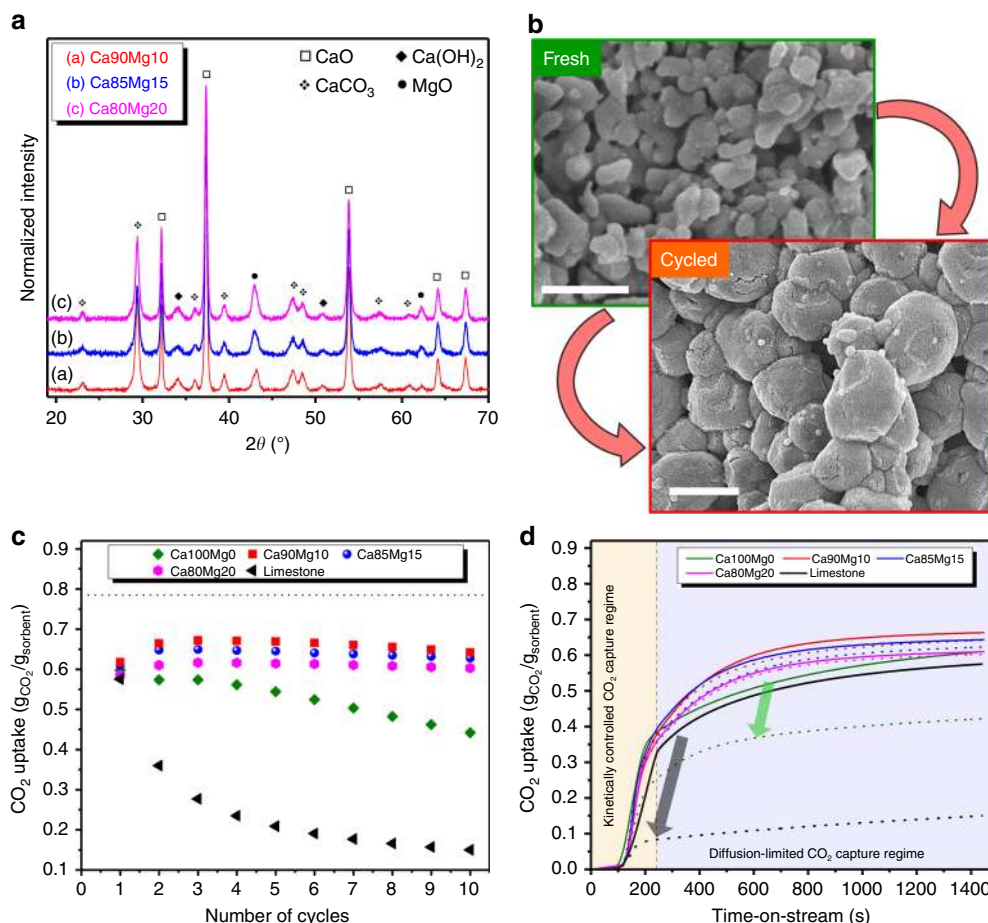

Fig. 4 Structure–performance relationship. **a** Powder XRD patterns of the sorbents synthesized after the removal of the carbonaceous template. **b** SEM images of the limestone-derived sorbent in the freshly calcined state and following ten operation cycles (scale bars: 400 nm). **c** CO$_2$ uptake of the hydrothermally synthesized CO$_2$ sorbents compared to limestone-derived CaO under harsh operating conditions (carbonation at 650 °C, calcination at 900 °C) (dotted line represents the maximum theoretical CO$_2$ uptake of Ca100Mg0). **d** Temporally resolved CO$_2$ uptake profiles of the hydrothermally synthesized sorbents in the 1st (solid line) and 10th (dashed line) carbonation cycle

of <100 nm in diameter and containing sufficient void space to accommodate the volumetric expansion of the material, will yield high CO_2 uptakes.

The influence of MgO on the performance of the sorbents was examined further by comparing the temporally resolved carbonation profiles of the different CO_2 sorbents (Fig. 4d). Indeed, all of the MgO-stabilized sorbents maintained their characteristic of capturing a large fraction of CO_2 in the kinetically controlled regime, in which surface reactions largely prevail (the overlapping CO_2 uptake curves in the early stages of the carbonation reaction indicate that the reaction in the TGA is dominated by mass transport from the bulk reactive gas to the outer surface of the sorbents). Importantly, the quantity of CO_2 captured by the MgO-stabilized sorbents in the initial reaction stage was maintained throughout the ten carbonation/calcination cycles (~0.35 $g_{CO_2}/g_{sorbent}$), whereas unstabilized CaO (Ca100Mg0) experienced an earlier transition to the diffusion-controlled CO_2 capture regime, decreasing the overall CO_2 uptake with increasing cycle number (from ~0.34 to 0.22 $g_{CO_2}/g_{sorbent}$). In Fig. 4d it can also be seen that the transition to the diffusion-controlled reaction stage occurred more gradually for MgO-stabilized sorbents, indicating that a larger pore volume was accessible in these materials. In contrast, the transition from the kinetically controlled to the diffusion-controlled carbonation stage was relatively sharp for limestone and Ca100Mg0, most likely owing to the blockage of narrow pores such that product layer diffusion became rate-limiting at much lower conversions when compared to MgO-stabilized sorbents[53].

It has been reported that the diffusion of CO_2 is enhanced in the presence of steam, a typical impurity in a flue gas stream[54,55]. Hence, we performed additional experiments using a mixture of N_2, CO_2 and steam (1.5–2 vol.%) during carbonation to assess the effect of steam on the new CO_2 sorbents (Supplementary Fig. 6). The presence of steam enhanced the apparent rate of CO_2 uptake significantly for both Ca85Mg15 and Ca80Mg20 and prevented an early transition to the diffusion-limited reaction stage. The total CO_2 uptake at the end of the 2nd carbonation reaction of Ca80Mg20 increased under wet conditions (i.e., 0.61 vs. 0.64 $g_{CO_2}/g_{sorbent}$ for dry vs. wet conditions, respectively), confirming the positive effect of steam on the performance of the sorbents.

Structure–performance relationship of the sorbents tested. Textural parameters, such as the specific surface area and pore volume, were determined by N_2 physisorption experiments in order to shed light on the structure–performance relationship of the materials (Supplementary Fig. 7 and Supplementary Table 1). In agreement with its cyclic performance, pure CaO obtained from freshly calcined limestone experiences a substantial drop in both its surface area (i.e., from 15 to 2 $m^2 g^{-1}$) and pore volume (i.e., from 0.168 to 0.009 $cm^3 g^{-1}$) after ten cycles of carbonation and calcination. When synthesized hydrothermally, pure CaO (i.e., Ca100Mg0) exhibited a higher pore volume after cyclic testing (i.e., 0.043 $cm^3 g^{-1}$), indicating that the porous multishelled morphology provided some level of thermal stability to the sorbent (Fig. 4c). Ca85Mg15, on the other hand, featured an even higher surface area and pore volume of 7 $m^2 g^{-1}$ and 0.084 cm^3/g (i.e., twice as high as Ca100Mg0 and nearly a tenfold increase compared to limestone), respectively, following ten operation cycles. Hence, it can be concluded that the presence of MgO plays a vital role in maintaining the favorable textural properties of the material. When the hydrothermal synthesis was performed in the absence of a carbonaceous template while keeping the Ca:Mg ratio constant at 85:15, the sorbent experienced decays of 93 and 83% in its surface area and pore volume, respectively, during cyclic operation. Similarly, natural dolomite,

which served as another reference material, lost more than 87% of its initial pore volume despite its high MgO content of more than 30 wt.%, suggesting that the presence of MgO per se does not suffice to preserve the initially high surface area and pore volume of the sorbent. In light of these observations, it can be concluded that both the presence of MgO and the porous, multishelled morphology of the sorbent are essential characteristics that are required simultaneously to enhance the CO_2 uptake performance of the material.

The stabilizing effect of MgO was revealed further by electron microscopy. SEM images given in Supplementary Fig. 8 confirm that the MgO-stabilized CO_2 sorbents undergo only minimal changes in their morphology. On the other hand, pure CaO microspheres "deform" and agglomerate from the first cycle onwards, leading in turn to a decrease in their CO_2 uptake. It is also noteworthy that the shells of the MgO-stabilized CO_2 sorbents possess an appreciable degree of porosity even in their carbonated state (Supplementary Fig. 8). This is in contrast to pure CaO microspheres, confirming further the favorable effect of the incorporation of high-T_T MgO to mitigate sintering and agglomeration of $CaCO_3$ during cyclic operation.

Performing ten repeated cycles of calcination and carbonation (Fig. 4c) did not suffice to capture in detail the minimum quantity of MgO required to ensure a stable cyclic behavior of the material. Therefore, MgO-stabilized sorbents were exposed to a higher number of CO_2 capture and regeneration cycles (Supplementary Fig. 9a). Capacity decays of 36.1, 17, and 17.1% were recorded for, respectively, Ca90Mg10, Ca85Mg15, and Ca80Mg20, outperforming limestone-derived CaO even more significantly (limestone lost more than 80% of its initial CO_2 uptake capacity after 30 cycles). The almost identical values of capacity retention for Ca85Mg15 and Ca80Mg20 indicate that increasing the MgO content beyond 15 mol% did not improve further the cyclic stability of the material (the addition of increasing quantities of MgO is ultimately a compromise between an increased structural stability of the material and a reduced quantity of CO_2 capture-active CaO). When the long-term performance of the sorbents was assessed under isothermal conditions at 750 °C (Supplementary Fig. 9b), MgO-stabilized sorbents featured a stable CO_2 uptake with a negligible capacity decay independent of their MgO content, whereas limestone-sorbent still lost more than half of its initial capacity even under such "mild" operating conditions.

The morphology of the best performing sorbent (i.e., Ca85Mg15) was probed by both FIB-SEM and STEM-EDX at different stages of the cyclic CO_2 capture and regeneration process (Fig. 5). SEM images of FIB cross-sections show the presence of a multishelled morphology of the as-synthesized CO_2 sorbents after the removal of the carbonaceous template. In addition to SEM images (Fig. 5a–c), both HAADF-STEM (Fig. 5d–f) and TEM (Supplementary Fig. 10) analyses confirm that the MgO-stabilized sorbents retain their favorable morphology, i.e., hollow spheres with highly porous shells, to a large extent during cyclic operation. This translates in turn to a cyclically stable CO_2 uptake. Furthermore, EDX maps of Ca and Mg (Fig. 5d–f) indicate that the homogeneous mixing between CaO and MgO at the nanometer scale persists not only in the carbonated state of the sorbent but also in the calcined state after ten operation cycles.

To capture the structural evolution of the hydrothermally synthesized sorbents during regeneration, in situ TEM was performed on Ca85Mg15 (carbonated state) by heating it up from room temperature to 1100 °C. As shown by the EDX maps of Ca, Mg, and O, provided in Fig. 6a, b, not only the multishelled structure, but also the compositional homogeneity of the sorbent was maintained, even at very high temperatures. It is also noteworthy that although the molar volume of $CaCO_3$ is twice as
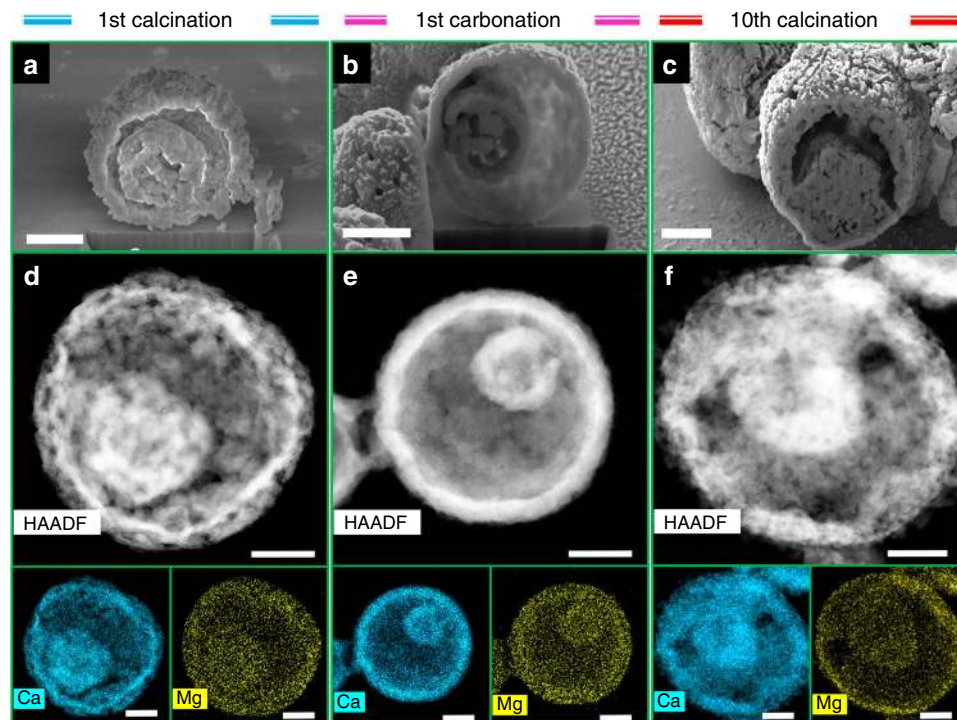
Fig. 5 Morphological changes during cyclic operation. **a–c** SEM images of FIB cross-sections. **d–f** HAADF-STEM images with EDX maps of Ca and Mg for Ca85Mg15 at different stages of CO_2 capture/regeneration cycles. Scale bars: 1 μm for **a–c** and 700 nm for **d–f**, respectively

high as that of CaO, the shrinkage in the diameter of the microsphere after being exposed to 1100 °C was determined to be <15% (Fig. 6c). Considering that the peak associated with carbon disappeared and the oxygen count dropped substantially in the EDX spectra at 1100 °C (Fig. 6d), the limited shrinkage cannot be related to an incomplete conversion of $CaCO_3$ to CaO, but rather to the favorable morphology of the sorbent, which provides sufficient void to accompany substantial volumetric changes during cyclic operations.

As demonstrated by the electron microscopy studies, the favorable structural features of the hydrothermally synthesized sorbents are preserved to a large extent over several CO_2 capture-regeneration cycles. The structural stability and compositional homogeneity of the material are believed to be the primary reasons for the cyclically stable performance of the CO_2 sorbents. To confirm this hypothesis and to probe in more detail the advantages of the template-assisted synthesis approach with regards to the morphology and CO_2 uptake of the material, alternative single-pot synthesis approaches were tested. These approaches that do not involve a template, include mechanical mixing or hydrothermal treatment in the absence of a carbon precursor. The ratio Ca:Mg was fixed to 85:15. In addition, calcined dolomite (a natural mineral with a nearly equimolar ratio of $MgCO_3$ and $CaCO_3$) served as a further reference material.

The cyclic CO_2 uptake performance of the additional sorbents synthesized is plotted in Fig. 7a, b. The sorbent prepared via the mechanical mixing of $CaCO_3$ and $MgCO_3$ exhibits a very similar trend as limestone-derived CaO, both in terms of CO_2 uptake and cyclic stability. Hence, the "simple" presence of a stabilizer (i.e., MgO) is not sufficient to yield a material with a high and cyclically stable CO_2 uptake. Electron microscopy of the sorbent prepared by mechanical mixing (Fig. 7c) reveals a rather ill-defined structure that is composed of comparatively large building blocks (>2 μm), pointing to the necessity of small particle sizes (both for the stabilizer and CaO) and a high degree

of porosity to yield a CO_2 sorbent that is superior to limestone. In addition, HAADF-STEM/EDX (Fig. 7d) along with SEM/EDX (Supplementary Fig. 11) confirms an inhomogeneous distribution of the stabilizer (MgO) within the active material (CaO) in both the as-synthesized and cycled material. This observation is an indication that also a homogeneous mixing between MgO and CaO (at the nanometer level) is critical for a structural stabilization and in turn, favorable CO_2 uptake characteristics.

The hydrothermally synthesized material without a carbonaceous template exhibits a slight improvement over the CO_2 uptake of its mechanically mixed counterpart (Fig. 7a, b), albeit revealing a significant capacity decay with cycle number. Interestingly, SEM images show that also this material has a rather ill-defined morphology that is composed of large particles (>2 μm) (Fig. 7c). The CO_2 uptake of the template-free material is appreciably lower than that of the CO_2 sorbents that were obtained via a template-assisted hydrothermal route. These observations suggest that, although the hydrothermal synthesis approach enables a compositional homogeneity between MgO and CaO as demonstrated by HAADF-STEM/EDX (Fig. 7d) and SEM/EDX analyses (Supplementary Fig. 12), a homogeneous mixing per se is not sufficient to yield a high and cyclically stable CO_2 uptake. Similarly, also dolomite contains a relatively homogeneous distribution of MgO nanoparticles within the CaO matrix (Supplementary Fig. 13), which is in line with previously reported studies[56,57]. Although dolomite-derived sorbents surpass the CO_2 uptake of their limestone-derived counterpart from the 4th cycle onward, the improvement was only marginal and the hydrothermally synthesized sorbents outperformed significantly dolomite (Fig. 7a). The notable capacity decay of dolomite-derived sorbents, despite their high content of MgO, can be explained by the segregation of MgO nanoparticles out of the CaO matrix, thereby losing their stabilizing role. This is visualized very well by electron microscopy (Supplementary Fig. 13).

These findings suggest that the presence of a void (providing the space required for the volume expansion during carbonation
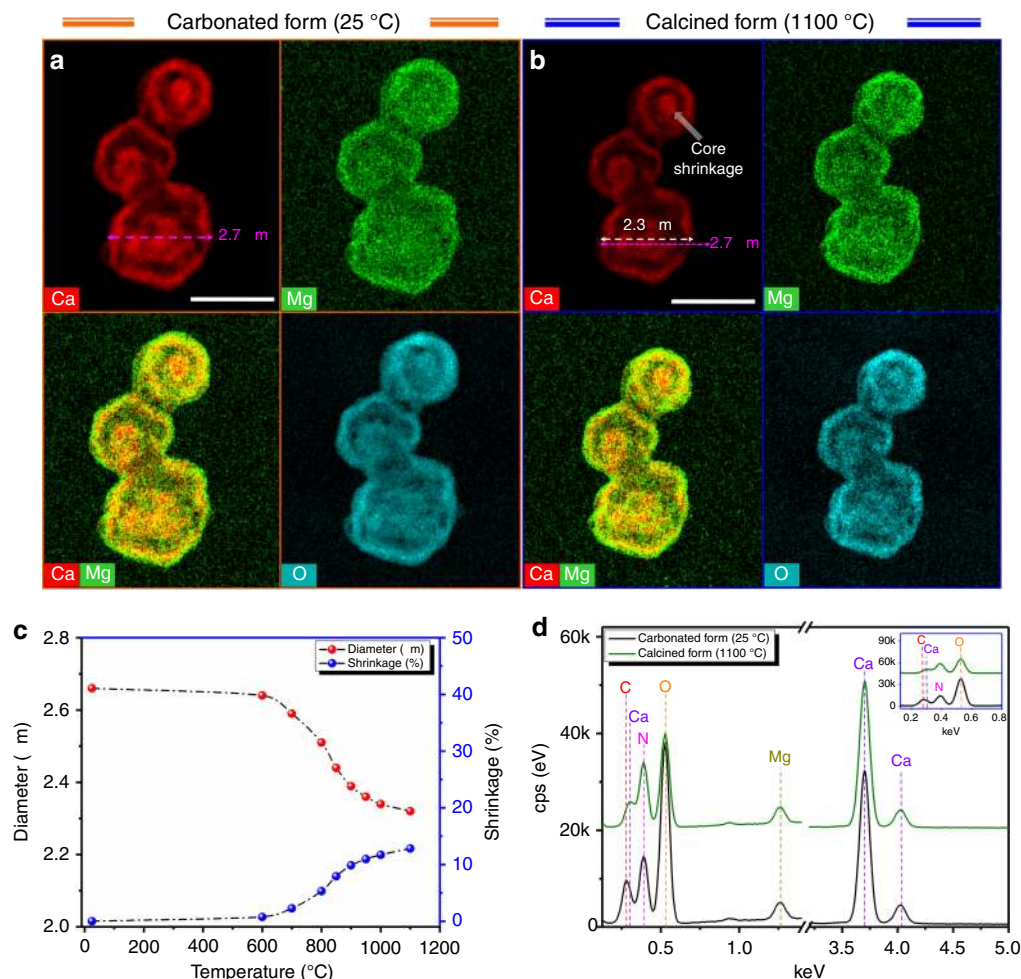
Fig. 6 Thermal stability of the multishelled structure. **a** STEM/EDX maps of Ca, Mg, and O in Ca85Mg15 acquired in carbonated form at room temperature. **b** STEM/EDX maps of Ca, Mg, and O in Ca85Mg15 acquired in calcined form at 1100 °C. **c** Change of the size of a microsphere as a function of temperature. **d** EDX spectra of Ca85Mg15 before and after calcination. Scale bars: 2 μm

and mitigating agglomeration and structural collapse) and limiting the size of the primary CaO particles to diameters <100 nm are features that are critical to obtain CaO-based materials with superior CO_2 uptake characteristics. Besides the macrostructure of the sorbents synthesized, XRD results reveal that the template also plays an important role in the crystallite size of CaO (Supplementary Fig. 14 and Supplementary Table 2). When synthesized hydrothermally in the presence of a carbonaceous template, the sorbents feature relatively small crystallite sizes of ~45 nm that is largely preserved over ten cycles (minor increase to ~48 nm). On the other hand, sorbents synthesized hydrothermally in the absence of a template had an initial crystallite size of ~73 nm and exceeded 100 nm after cyclic operation. As a final note, when we replaced xylose by other inexpensive and widely available carbon precursors (i.e., glucose), materials with similar morphologies (Supplementary Fig. 15) and comparable CO_2 uptakes (Fig. 7a) were obtained.

Discussion

In summary, we report a facile one-pot synthesis approach to yield highly effective, MgO-stabilized, CaO-based CO_2 sorbents. When mixed homogeneously with CaO on the nanometer level, MgO acts as an inert, sintering retarding structural stabilizer. The presence of a carbonaceous template during synthesis allowed (after its removal) for the formation of a well-defined morphology featuring multishelled structures with a high degree of porosity; a

critical requirement for a high CO_2 uptake. By assessing alternative synthesis approaches, we demonstrate that the compositional homogeneity and the formation of a (multi)shelled morphology, containing excess porosity and being composed of small nanoparticles, are key requirements that have to be met to obtain effective CO_2 sorbents. Using a template-assisted hydrothermal approach, a MgO content of as little as 15 mol% (i.e., 11 wt.%) is sufficient to obtain a high level of cyclic stability. The best sorbent retained 83% of its initial CO_2 uptake over 30 CO_2 capture and regeneration cycles under practically relevant operating conditions, outperforming the limestone-derived benchmark by ~500%.

Methods

Synthesis protocol for the sorbents. MgO-stabilized, multishelled CaO-based microspheres were synthesized via a hydrothermal approach. In a typical synthesis, D-(+)-xylose (40 mmol; Sigma Aldrich) and glycine (6.6 mmol; Acros Organics) were dissolved in 15 ml of deionized (DI) water under vigorous stirring for 10 min. Next, calcium and magnesium precursors, i.e., $Ca(NO_3)_2 \cdot 4H_2O$ and $Mg(NO_3)_2 \cdot 6H_2O$ (from Acros Organics) were added in appropriate quantities (in total 17 mmol with different molar ratios of Ca:Mg of 90:10, 85:15, and 80:20) to the xylose solution under vigorous stirring. After mixing for 10 min, 3 ml of an aqueous urea solution (2 M) was introduced to the reaction mixture. Following vigorous stirring for 5 min, the solution was transferred to a 45-ml Teflon-lined stainless-steel autoclave. The autoclave was kept in an oven at 180 °C for 24 h. After cooling down to room temperature, a black, powdery material was collected by filtration and washed thoroughly with DI water and ethanol. Drying of the filtrate at 80 °C overnight and subsequent calcination in a muffle furnace at 800 °C for 2 h (5 °C min^{-1} ramp rate) yielded the final CO_2 sorbent. For comparison, samples
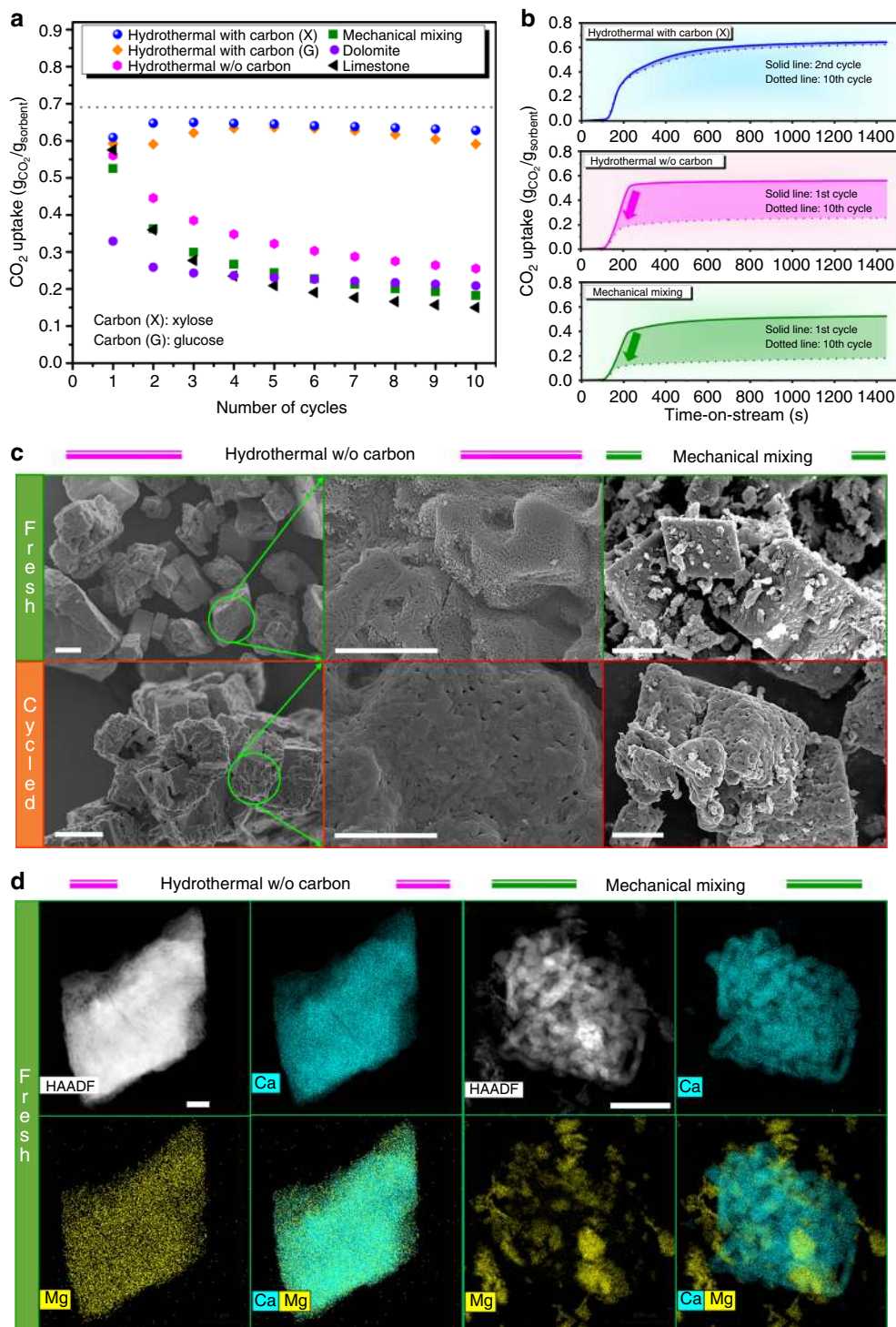
Fig. 7 Effect of the synthesis approach on performance and structure. **a** CO_2 uptake over ten cycles of calcination and carbonation of CO_2 sorbents that contain a molar ratio of Ca:Mg = 85:15 synthesized by two different approaches: hydrothermal versus mechanical mixing (dotted line represents the maximum theoretical CO_2 uptake of Ca85Mg15). **b** Temporally resolved carbonation profiles of the sorbents with the highest and lowest CO_2 uptakes. **c**, **d** SEM images of the as-synthesized and cycled materials, and HAADF-STEM image and EDX mapping of the as-synthesized materials prepared by a hydrothermal route in the absence of a carbon precursor and by mechanical mixing of $CaCO_3$ and $MgCO_3$. Scale bars in **c**: 20 μm for the 1st column and 2 μm for the 2nd and 3rd columns, respectively. Scale bars: 500 nm in **d**

with the aforementioned Ca:Mg molar ratios were also prepared by mechanical mixing of $CaCO_3$ and $MgCO_3$. Following the mechanical mixing of appropriate amounts of $CaCO_3$ and $MgCO_3$ for 20 min, the samples were calcined in a muffle furnace at 800 °C for 2 h (5 °C min⁻¹ ramp rate).

For simplicity, the following nomenclature is used to describe the composition of the CO_2 sorbents throughout the text: The elemental abbreviations ("Ca" and "Mg" for CaO and MgO, respectively) are followed by a number that quantifies the

molar composition of the sorbent. For example, the sorbent Ca85Mg15 contains a molar ratio of Ca:Mg of 85:15.

Performance characterization. The cyclic CO_2 uptake of the sorbents synthesized was evaluated in a thermogravimetric analyzer (TGA, Mettler Toledo TGA/DSC 1) at atmospheric pressure. A ramping rate of 50 °C min⁻¹ was used for all heating

and cooling cycles. The sample (typically ~5 mg) was loaded in a 70-μl alumina crucible and heated to 900 °C under a nitrogen flow (120 ml min^{-1} including the constant purge flow of 25 ml min^{-1} over the microbalance). After calcination (5 min), the sample was cooled down to 650 °C and the cyclic test started with the carbonation reaction (20 vol.% CO_2 in N_2 for 20 min). Following carbonation, the sorbent was regenerated by increasing the temperature to 900 °C in a CO_2 atmosphere. To ensure a complete regeneration of the sorbent, the sample was maintained at 900 °C for 10 min. These calcination and carbonation steps were repeated for the desired number of cycles. Throughout the operation, the weight change of the sorbent was continuously monitored and recorded.

N$_2$ physisorption. N_2 physisorption experiments were performed in a NOVA 4000e analyzer (Quantachrome Instruments). The adsorption and desorption of N_2 were determined at −196 °C. Prior to the N_2 physisorption measurements, the samples were degassed under vacuum at 300 °C for at least 3 h. Brunauer–Emmett–Teller (BET) and Barrett–Joyner–Halenda (BJH) models were used to calculate, respectively, the surface area and the pore-size distribution of the materials.

X-ray diffraction. Powder XRD (Bruker, AXS D8 Advance) was utilized to investigate the crystallinity and the chemical composition of the materials synthesized. The diffractometer was equipped with a super-speed Lynxeye detector which was operated at 40 mA and 40 kV (2θ range of 10–90° with a step size of 0.025° and a step duration of 0.8 s). Rietveld refinement analysis of the XRD patterns was performed using FullProf. The average crystallite sizes (D) of CaO and MgO were estimated using the Scherrer Eq. (2):

$$D = \frac{K\lambda}{\beta \cos\theta} \qquad (2)$$

where K is the shape factor (i.e., 0.9 for a spherical particle), λ is the wavelength of the X-ray radiation used (0.15418 nm), β is the full width at half maximum intensity (FWHM), and θ is the Bragg angle (peak position) of the corresponding reflection.

ICP-OES. Inductively coupled plasma–optical emission spectroscopy (ICP-OES) was performed on a Varian 720-ES. For calibration, the multi-element standard 5 (Sigma Aldrich) was used. Samples were prepared by treating ~3 mg of the sample with 4 ml of aqua regia (3:1 HCl:HNO$_3$). The resulting solutions were diluted with DI water to yield a volume of 25 ml. To avoid any contamination, trace-grade acids (HCl and HNO$_3$), and HNO$_3$-leached glassware were used.

Electron microscopy. A high-resolution field-emission SEM (Zeiss ULTRA 55 plus) was utilized to visualize the materials. Prior to imaging, the samples were sputter-coated (BAL-TEC SCD-050) with Au/Pd to improve their conductivity. For the elemental mapping of Ca and Mg, a Leo Gemini 1530 equipped with an EDX detector was used.

Cross-sections of the synthesized microspheres were prepared by focused ion beam (FIB) equipped with a Ga liquid metal ion source and imaged with a high-resolution FE-SEM (Zeiss, FIB-SEM NVision 40). Prior to FIB-SEM analysis, the samples were dispersed and stabilized on a Si wafer.

The microstructure of the materials was probed by TEM (FEI Talos F200X) equipped with a high-brightness field-emission gun, a high-angle annular dark field (HAADF) detector, and a large collection-angle EDX detector. The operation voltage of the instrument was set to 200 kV in both TEM and scanning TEM (STEM) modes. For the ex situ analysis of the samples, the powders were dispersed onto Cu grids coated with lacey carbon.

For the in situ heating experiments, the sample was dispersed onto MEMS chips with SiN$_x$ windows (Wildfire D6, DENSsolutions). The sample was heated up from 25 to 1100 °C at a ramp rate of 50 °C min^{-1} and then rapidly cooled down to room temperature.

References

1. Gibbins, J. & Chalmers, H. Carbon capture and storage. *Energy Policy* **36**, 4317–4322 (2008).
2. Boot-Handford, M. E. et al. Carbon capture and storage update. *Energy Environ. Sci.* **7**, 130–189 (2014).
3. Betts, R. A., Jones, C. D., Knight, J. R., Keeling, R. F. & Kennedy, J. J. El Niño and a record CO_2 rise. *Nat. Clim. Change* **6**, 806–810 (2016).
4. Zhou, F. et al. Ultrathin graphene oxide-based hollow fiber membranes with brush-like CO_2-philic agent for highly efficient CO_2 capture. *Nat. Commun.* **8**, 2107 (2017).
5. Liang, L. et al. Carbon dioxide capture and conversion by an acid-base resistant metal-organic framework. *Nat. Commun.* **8**, 1233 (2017).
6. Fu, Y. et al. Ultra-thin enzymatic liquid membrane for CO_2 separation and capture. *Nat. Commun.* **9**, 990 (2018).
7. Tuinier, M. J., Hamers, H. P., & van SInt Annaland, M. Techno-economic evaluation of cryogenic CO_2 capture'A comparison with absorption and membrane technology. *Int. J. Greenh. Gas Control* **5**, 1559–1565 (2011).
8. Yu, K., Mitch, W. A. & Dai, N. Nitrosamines and nitramines in amine-based carbon dioxide capture systems: fundamentals, engineering implications, and knowledge gaps. *Environ. Sci. Technol.* **51**, 11522–11536 (2017).
9. Vericella, J. J. et al. Encapsulated liquid sorbents for carbon dioxide capture. *Nat. Commun.* **6**, 6124 (2015).
10. Choi, S., Drese, J. H. & Jones, C. W. Adsorbent materials for carbon dioxide capture from large anthropogenic point sources. *ChemSusChem* **2**, 796–854 (2009).
11. Kierzkowska, A. M., Pacciani, R. & Müller, C. R. CaO-based CO_2 sorbents: from fundamentals to the development of new, highly effective materials. *ChemSusChem* **6**, 1130–1148 (2013).
12. Wang, J. et al. Recent advances in solid sorbents for CO_2 capture and new development trends. *Energy Environ. Sci.* **7**, 3478–3518 (2014).
13. Hanak, D. P., Anthony, E. J. & Manovic, V. A review of developments in pilot-plant testing and modelling of calcium looping process for CO_2 capture from power generation systems. *Energy Environ. Sci.* **8**, 2199–2249 (2015).
14. Erans, M., Manovic, V. & Anthony, E. J. Calcium looping sorbents for CO_2 capture. *Appl. Energy* **180**, 722–742 (2016).
15. Su, C., Duan, L., Donat, F. & Anthony, E. J. From waste to high value utilization of spent bleaching clay in synthesizing high-performance calcium-based sorbent for CO_2 capture. *Appl. Energy* **210**, 117–126 (2018).
16. Liu, W. et al. Performance enhancement of calcium oxide sorbents for cyclic CO_2 capture-a review. *Energy Fuels* **26**, 2751–2767 (2012).
17. Naeem, M. A., Armutlulu, A., Broda, M., Lebedev, D. & Müller, C. R. The development of effective CaO-based CO_2 sorbents via a sacrificial templating technique. *Faraday Disc.* **192**, 85–95 (2016).
18. Feng, J., Guo, H., Wang, S., Zhao, Y. & Ma, X. Fabrication of multi-shelled hollow Mg-modified CaCO$_3$ microspheres and their improved CO_2 adsorption performance. *Chem. Eng. J.* **321**, 401–411 (2017).
19. Naeem, M. A., Armutlulu, A., Imtiaz, Q. & Müller, C. R. CaO-based CO_2 sorbents effectively stabilized by metal oxides. *Chemphyschem* **18**, 3280–3285 (2017).
20. Armutlulu, A. et al. Multishelled CaO microspheres stabilized by atomic layer deposition of Al$_2$O$_3$ for enhanced CO_2 capture performance. *Adv. Mater.* **29**, 1702896 (2017).
21. Han, R., Gao, J., Wei, S., Su, Y. & Qin, Y. Development of highly effective CaO@Al$_2$O$_3$ with hierarchical architecture CO_2 sorbents via a scalable limited-space chemical vapor deposition technique. *J. Mater. Chem. A* **6**, 3462–3470 (2018).
22. Broda, M., Kierzkowska, A. M. & Müller, C. R. Development of highly effective CaO-based, MgO-stabilized CO_2 sorbents via a scalable "one-pot" recrystallization technique. *Adv. Funct. Mater.* **24**, 5753–5761 (2014).
23. Kim, S. M. et al. In situ XRD and dynamic nuclear polarization surface enhanced NMR spectroscopy unravel the deactivation mechanism of CaO-based, Ca$_3$Al$_2$O$_6$-stabilized CO_2 sorbents. *Chem. Mater.* **30**, 1344–1352 (2018).
24. Li, P., Liu, W., Dennis, J. S. & Zeng, H. C. Synthetic architecture of MgO/C nanocomposite from hierarchical-structured coordination polymer toward enhanced CO_2 capture. *ACS Appl. Mater. Interfaces* **9**, 9592–9602 (2017).
25. Wang, S., Yan, S., Ma, X. & Gong, J. Recent advances in capture of carbon dioxide using alkali-metal-based oxides. *Energy Environ. Sci.* **4**, 3805–3819 (2011).
26. Manovic, V. & Anthony, E. J. Steam reactivation of spent CaO-based sorbent for multiple CO_2 capture cycles. *Environ. Sci. Technol.* **41**, 1420–1425 (2007).
27. Wang, H., Li, Z., Fan, X. & Cai, N. Rate-equation-based grain model for the carbonation of CaO with CO_2. *Energy Fuels* **31**, 14018–14032 (2017).
28. Alvarez, D. & Abanades, J. C. Determination of the critical product layer thickness in the reaction of CaO with CO_2. *Ind. Eng. Chem. Res.* **44**, 5608–5615 (2005).
29. Li, Z.-S., Fang, F., Tang, X.-Y. & Cai, N.-S. Effect of temperature on the carbonation reaction of CaO with CO_2. *Energy Fuels* **26**, 2473–2482 (2012).
30. Martavaltzi, C. S. & Lemonidou, A. A. Parametric study of the CaO–Ca$_{12}$Al$_{14}$O$_{33}$ synthesis with respect to high CO_2 sorption capacity and stability on multicycle operation. *Ind. Eng. Chem. Res.* **47**, 9537–9543 (2008).
31. Liu, W. et al. Synthesis of sintering-resistant sorbents for CO_2 capture. *Environ. Sci. Technol.* **44**, 3093–3097 (2010).
32. Florin, N. H., Blamey, J. & Fennell, P. S. Synthetic CaO-based sorbent for CO_2 capture from large-point sources. *Energy Fuels* **24**, 4598–4604 (2010).

33. Li, L., King, D. L., Nie, Z. & Howard, C. Magnesia-stabilized calcium oxide absorbents with improved durability for high temperature CO_2 capture. *Ind. Eng. Chem. Res.* **48**, 10604–10613 (2009).

34. Angeli, S. D., Martavaltzi, C. S. & Lemonidou, A. A. Development of a novel-synthesized Ca-based CO_2 sorbent for multicycle operation: parametric study of sorption. *Fuel* **127**, 62–69 (2014).

35. Lu, H., Khan, A., Pratsinis, S. E. & Smirniotis, P. G. Flame-made durable doped-CaO nanosorbents for CO_2 capture. *Energy Fuels* **23**, 1093–1100 (2009).

36. Chang, P. H., Chang, Y. P., Chen, S. Y., Yu, C. T. & Chyou, Y. P. Ca-rich Ca–Al-oxide, high-temperature-stable sorbents prepared from hydrotalcite precursors: synthesis, characterization, and CO_2 capture capacity. *ChemSusChem* **4**, 1844–1851 (2011).

37. Wang, S., Li, C., Yan, S., Zhao, Y. & Ma, X. Adsorption of CO_2 on mixed oxides derived from Ca–Al–ClO_4-layered double hydroxide. *Energy Fuels* **30**, 1217–1222 (2016).

38. Radfarnia, H. R. & Sayari, A. A highly efficient CaO-based CO_2 sorbent prepared by a citrate-assisted sol–gel technique. *Chem. Eng. J.* **262**, 913–920 (2015).

39. Liu, F.-Q., Li, W.-H., Liu, B.-C. & Li, R.-X. Synthesis, characterization, and high temperature CO_2 capture of new CaO based hollow sphere sorbents. *J. Mater. Chem. A* **1**, 8037–8044 (2013).

40. Titirici, M.-M., Antonietti, M. & Thomas, A. A generalized synthesis of metal oxide hollow spheres using a hydrothermal approach. *Chem. Mater.* **18**, 3808–3812 (2006).

41. Qi, J. et al. Multi-shelled hollow micro-/nanostructures. *Chem. Soc. Rev.* **44**, 6749–6773 (2015).

42. Caruso, F., Caruso, R. A. & Möhwald, H. Nanoengineering of inorganic and hybrid hollow spheres by colloidal templating. *Science* **282**, 1111–1114 (1998).

43. Caruso, F., Spasova, M., Susha, A., Giersig, M. & Caruso, R. A. Magnetic nanocomposite particles and hollow spheres constructed by a sequential layering approach. *Chem. Mater.* **13**, 109–116 (2001).

44. Li, Y. & Shi, J. Hollow-structured mesoporous materials: chemical synthesis, functionalization and applications. *Adv. Mater.* **26**, 3176–3205 (2014).

45. Cui, X., Antonietti, M. & Yu, S. H. Structural effects of iron oxide nanoparticles and iron ions on the hydrothermal carbonization of starch and rice carbohydrates. *Small* **2**, 756–759 (2006).

46. Wang, S. et al. CaO-based meshed hollow spheres for CO_2 capture. *Chem. Eng. Sci.* **135**, 532–539 (2015).

47. Staal, L. B. et al. Competitive reactions during synthesis of zinc aluminum layered double hydroxides by thermal hydrolysis of urea. *J. Mater. Chem. A* **5**, 21795–21806 (2017).

48. Prevot, V., Caperaa, N., Taviot-Guého, C. & Forano, C. Glycine-assisted hydrothermal synthesis of NiAl-layered double hydroxide nanostructures. *Cryst. Growth Des.* **9**, 3646–3654 (2009).

49. Titirici, M.-M., Antonietti, M. & Baccile, N. Hydrothermal carbon from biomass: a comparison of the local structure from poly-to monosaccharides and pentoses/hexoses. *Green Chem.* **10**, 1204–1212 (2008).

50. ElKhatat, A. M. & Al-Muhtaseb, S. A. Advances in tailoring resorcinol-formaldehyde organic and carbon gels. *Adv. Mater.* **23**, 2887–2903 (2011).

51. Hu, Y. et al. Screening of inert solid supports for CaO-based sorbents for high temperature CO_2 capture. *Fuel* **181**, 199–206 (2016).

52. Lai, X. et al. General synthesis and gas-sensing properties of multiple-shell metal oxide hollow microspheres. *Angew. Chem. Int. Ed.* **123**, 2790–2793 (2011).

53. Alvarez, D. & Abanades, J. C. Pore-size and shape effects on the recarbonation performance of calcium oxide submitted to repeated calcination/recarbonation cycles. *Energy Fuels* **19**, 270–278 (2005).

54. Donat, F., Florin, N. H., Anthony, E. J. & Fennell, P. S. Influence of high-temperature steam on the reactivity of CaO sorbent for CO_2 capture. *Environ. Sci. Technol.* **46**, 1262–1269 (2012).

55. Li, Z., Liu, Y. & Cai, N. Understanding the enhancement effect of high-temperature steam on the carbonation reaction of CaO with CO_2. *Fuel* **127**, 88–93 (2014).

56. Valverde, J., Sanchez-Jimenez, P. & Perez-Maqueda, L. Ca-looping for postcombustion CO_2 capture: a comparative analysis on the performances of dolomite and limestone. *Appl. Energy* **138**, 202–215 (2015).

57. de la Calle Martos, A. et al. Effect of dolomite decomposition under CO_2 on its multicycle CO_2 capture behaviour under calcium looping conditions. *Phys. Chem. Chem. Phys.* **18**, 16325–16336 (2016).

Acknowledgements

Author contributions

C.R.M. conceived the project and designed the experiments with M.A.N. and A.A., M.A.N. synthesized the sorbents, evaluated their performance in a TGA with the help of F.D., and characterized their structure via XRD., M.A.N. and A.A. carried out N_2 physisorption experiments. A.A. performed FIB, SEM, and SEM/EDX experiments. A.A. and Q.I. conducted TEM, STEM, and STEM/EDX analysis. A.A. and R.S. performed the in situ TEM experiments. A.K. performed ICP-OES. All authors contributed to discussions. M.A.N., A.A., and C.R.M. wrote the manuscript with contributions from all authors. C.R.M. supervised the work.

Additional information